Realizations of highly heterogeneous collagen networks via stochastic reconstruction for micromechanical analysis of tumor cell invasion

Hanqing Nan,[1] Long Liang,[2] Guo Chen,[3] Liyu Liu,[3] Ruchuan Liu,[3,*] and Yang Jiao[1,2,†]
[1]*Materials Science and Engineering, Arizona State University, Tempe, Arizona 85287, USA*
[2]*Department of Physics, Arizona State University, Tempe, Arizona 85287, USA*
[3]*College of Physics, Chongqing University, Chongqing 401331, China*

(Received 21 December 2017; revised manuscript received 25 February 2018; published 21 March 2018)

Three-dimensional (3D) collective cell migration in a collagen-based extracellular matrix (ECM) is among one of the most significant topics in developmental biology, cancer progression, tissue regeneration, and immune response. Recent studies have suggested that collagen-fiber mediated force transmission in cellularized ECM plays an important role in stress homeostasis and regulation of collective cellular behaviors. Motivated by the recent *in vitro* observation that oriented collagen can significantly enhance the penetration of migrating breast cancer cells into dense Matrigel which mimics the intravasation process *in vivo* [Han *et al.* Proc. Natl. Acad. Sci. USA **113**, 11208 (2016)], we devise a procedure for generating realizations of highly heterogeneous 3D collagen networks with prescribed microstructural statistics via stochastic optimization. Specifically, a collagen network is represented via the graph (node-bond) model and the microstructural statistics considered include the cross-link (node) density, valence distribution, fiber (bond) length distribution, as well as fiber orientation distribution. An optimization problem is formulated in which the objective function is defined as the squared difference between a set of target microstructural statistics and the corresponding statistics for the simulated network. Simulated annealing is employed to solve the optimization problem by evolving an initial network via random perturbations to generate realizations of homogeneous networks with randomly oriented fibers, homogeneous networks with aligned fibers, heterogeneous networks with a continuous variation of fiber orientation along a prescribed direction, as well as a binary system containing a collagen region with aligned fibers and a dense Matrigel region with randomly oriented fibers. The generation and propagation of active forces in the simulated networks due to polarized contraction of an embedded ellipsoidal cell and a small group of cells are analyzed by considering a nonlinear fiber model incorporating strain hardening upon large stretching and buckling upon compression. Our analysis shows that oriented fibers can significantly enhance long-range force transmission in the network. Moreover, in the oriented-collagen-Matrigel system, the forces generated by a polarized cell in collagen can penetrate deeply into the Matrigel region. The stressed Matrigel fibers could provide contact guidance for the migrating cell cells, and thus enhance their penetration into Matrigel. This suggests a possible mechanism for the observed enhanced intravasation by oriented collagen.

DOI: 10.1103/PhysRevE.97.033311

I. INTRODUCTION

The extracellular matrix (ECM) is an interconnected network of biopolymers mainly composed of type I collagen that provides structural support for cells and allows the diffusion of biochemicals within tissues [1]. Cells attach to and move through the ECM using protein complexes that link the ECM to the force-generating cell cytoskeleton [2]. These cell-ECM adhesions also act as sensors, allowing cells to respond to the local microstructure and mechanical properties of the surrounding ECM [3,4] and regulating various cell behaviors [5–7]. For example, the stiffness and alignment of collagen fibers in the ECM can significantly affect cellular migration [8,9], via durotaxis (i.e., cells tend move in the direction of increasing matrix stiffness) [10] and contact guidance (i.e., cells tend to move in the direction of fiber alignment) [11,12].

On the other hand, active cells can remodel the network [4,13,14] and even affect the bulk properties of the ECM [15–18]. Specifically, tension exerted by the cells can align the fibers in the network leading to long range force transmission [15,19–22]. Fiber mediated stresses can in turn trigger mechanosensitive pathways for regulating collective cell dynamics [23–29]. This coupling of cells provides a means for mechanical communication and plays an important role in regulating and coordinating collective cellular dynamics in a wide range of biophysical processes, such as morphogenesis, tissue regeneration, and immune response, as well as diseases such as muscular dystrophy, fibrosis, and cancer [4,13,30–34].

A significant amount of work has been carried out to characterize the microstructural [35–46] and physical properties [15,17–19,23,42,45,47–66] of the collagen networks as well as cellularized ECM systems [67–69]. In addition, a variety of discrete fiber-based models have been devised to investigate the mechanical behavior and force transmission in biopolymer networks [15,21,22,66,70–75]. In such models, the collagen gel is typically treated as a semiflexible network [76] and

*phyliurc@cqu.edu.cn
†yang.jiao.2@asu.edu

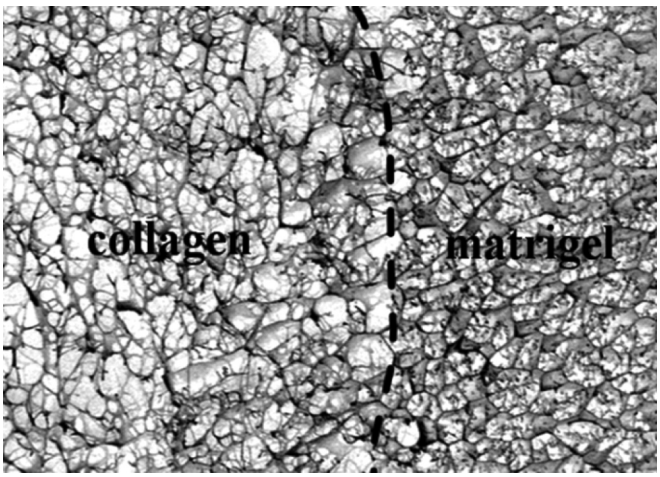

FIG. 1. SEM (scanning electron microscopy) image showing the microstructure of the model heterogeneous ECM which contains a collagen region (upper part) attached to a layer of dense Matrigel (lower part).

represented using a graph (i.e., bond-node) model in which each bond represents a fiber segment and a node represents a possible cross link. It is found that the fibreous nature and nonlinear mechanical response of the collagen fibers can support long-range force transmission [21,22,66,74,77,78] and thus, suggests a possible mechanism for long-range mechanical signaling between distant cells [79,80]. Interesting, the propagation of mechanical forces due to local perturbations in collagen networks share some similarity to that in disordered granular materials [81,82].

In spite of the exciting progress in understanding the dynamic cell-ECM interactions, the effects of microstructural heterogeneity of the ECM have not been systematically investigated. The preponderance of the aforementioned studies has employed relatively simple model networks with artificial geometrical or topological disorder. Recently, a stochastic reconstruction method has been devised that allows one to generate virtual collagen networks possessing prescribed local topological and geometrical statistics associated with actual collagen networks [45]. Such statistics include the valence number distribution (i.e., the number of fibers at a cross-link node), fiber length distribution, and fiber orientation (i.e., direction cosine) direction, which can be computed from 3D confocal images of the network of interest. However, the reconstructed virtual networks are spatially homogeneous, i.e., the prescribed statistics are invariant at different locations of the systems, which might not fully capture the heterogeneous nature of the *in vivo* microenvironment.

Very recently, an *in vitro* model of 3D heterogeneous ECM containing metastatic breast cancer (MDA-MB-231) cells have been constructed in order to investigate the effect of ECM heterogeneity on cancer invasion [83]. The model ECM contains a collagen region with either randomly orientated or aligned collagen fibers, which is attached to a layer of dense Matrigel (see Fig. 1). This is to mimic the stroma surrounding a breast tumor which includes both remodeled collagens as well as dense basal membranes. As the first step for leaving the primary tumor and entering into the circulation system, the invasive cells need to penetrate the dense basal membranes. It has been shown in this *in vitro model* the tumor cells in the ECM with prealigned fibers can easily penetrate deeply into the dense Matrigel region, while the same cells in random ECM cannot. This observation has led to the conclusion that oriented collagen fibers can significantly enhance tumor cell intravasation. However, the mechanism for this new paradigm is not fully understood yet.

As a first step towards a better understanding of the mechanisms underlying the enhanced tumor cell intravasation by aligned collagen fibers, we develop a procedure for generating realizations of highly heterogeneous 3D collagen networks with prescribed microstructural statistics via stochastic optimization, which generalizes the framework devised in Ref. [45]. We note that ECM is an intrinsic heterogeneous material. For example, the local cross-link (node) density, the coordination (valence) number at each node, and the fiber orientations are all varying at different locations of the system. By "highly heterogeneous," we mean that besides the intrinsic spatial variation of the aforementioned local properties, the system also includes large and abrupt changes of local properties (e.g., the fiber orientations) as observed in the *in vitro* ECM constructed in Ref. [83]. In this work, a collagen network is represented via the graph (node-bond) model and the microstructural statistics considered include the *spatial-location dependent* cross-link (node) density, valence distribution, fiber (bond) length distribution, as well as fiber orientation distribution. An optimization problem is formulated in which the objective function is defined as the squared difference between a set of target microstructural statistics and the corresponding statistics for the simulated network. Simulated annealing is employed to solve the optimization problem by evolving an initial network via random perturbations in order to match the specific statistics in different regions of the system to generate realizations of desirable networks.

We first employ this procedure to render realizations of homogeneous networks with randomly oriented fibers, homogeneous networks with aligned fibers, heterogeneous networks with a continuous variation of fiber orientation along a prescribed direction, as well as a binary system containing a collagen region with aligned fibers and a dense Matrigel region with randomly oriented fibers. Subsequently, the generation and propagation of active forces in the virtual ECM networks due to polarized contraction of an embedded ellipsoidal cell are analyzed by considering a nonlinear fiber model. Specifically, the fiber's constitutive relation incorporates strain hardening upon large stretching and buckling upon compression. Our analysis shows that oriented fibers can significantly enhance long-range force transmission in the network. Moreover, in the oriented-collagen-Matrigel system, the forces generated by a polarized cell in collagen can penetrate deeply into the Matrigel region. Such stressed Matrigel fibers could provide contact guidance for the migrating cells, and thus enhance their penetration into Matrigel. This suggests a possible mechanism for the observed enhanced intravasation by oriented collagen. We also investigate the propagation of active forces generated by a small group of cells in the ECM with varying degree of heterogeneities, to mimic the collective contraction of the invasion front of the *in vitro* tumor.

The rest of the paper is organized as follows: In Secs. II and III we, respectively, describe the formulation of the stochastic reconstruction procedure and the micromechanical model for cell-ECM mechanical interaction analysis. In Sec. IV we report our reconstruction results for various virtual ECM networks including the highly heterogeneous ECM that mimics the *in vitro* microenvironment reported in Ref. [83]. In Sec. V we carry out detailed micromechanical analysis of the effects of the ECM heterogeneity in active force propagation during tumor cell invasion. In Sec. VI we provide concluding remarks.

II. STOCHASTIC RECONSTRUCTION PROCEDURE

A. General reconstruction procedure for homogeneous networks

Our general reconstruction procedure follows closely that devised in Ref. [45] and is based on the stochastic-optimization material reconstruction method originally developed by Yeong and Torquato [84,85] and subsequently generalized to model a wide spectrum of heterogeneous systems [86–96].

Specifically, consider a 3D collagen-based ECM network $\mathbb{M}$ represented by the graph (node-bond) model, in which each bond represents a collagen fiber segment and each node represents a cross link (see Fig. 2). The network microstructure is statistically characterized by the statistics set $\mathbb{D}$. In the work we consider the following statistics set:

$$\mathbb{D} = \{c_0, \mathbf{n}, \mathbf{L}, \Omega\}, \tag{1}$$

where c_0 is the node number density, $\mathbf{n}$ is the distribution of valence number (i.e., the number of fibers that a node is connected to), $\mathbf{L}$ is the length distribution of the fibers, and Ω is the distribution of the fiber orientation with respect to the z axis. Such structural statistics can be obtained either from 3D confocal images of the ECM or from theoretical considerations, and are spatially invariant for a homogeneous network.

Generally, a formal mathematical transformation $\mathscr{F}$ can be defined that maps a network $\mathbb{M}$ to the statistics data set $\mathbb{D}$, i.e.,

$$\mathbb{D} = \mathscr{F}[\mathbb{M}]. \tag{2}$$

The reconstruction is formulated as the inverse problem in which a realization of $\mathbb{M}$ is rendered from a given data set $\mathbb{D}$,

$$\mathbb{M} = \mathscr{F}^{-1}[\mathbb{D}]. \tag{3}$$

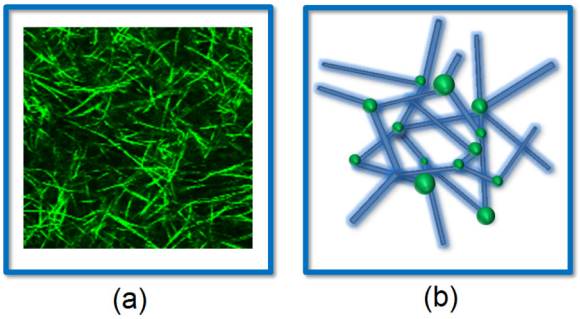

FIG. 2. Schematic illustration of the bond-node mode (b) for a collagen network derived from its confocal image (a).

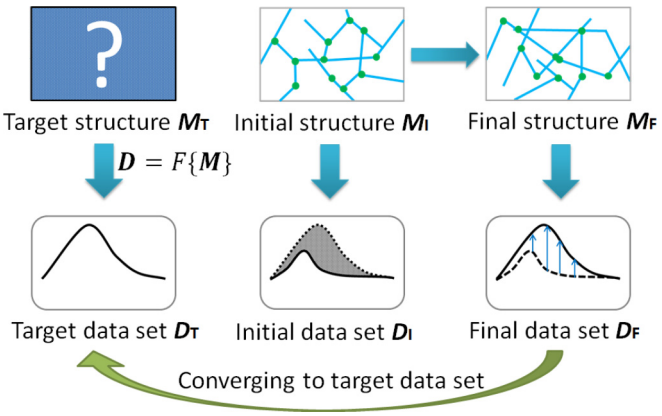

FIG. 3. Schematic illustration of the overall network reconstruction procedure based on stochastic optimization.

Here we employ the simulated annealing procedure [97] to solve the reconstruction problem, which is formulated as an optimization problem. Specifically, for an unknown "target" network configuration $\mathbb{M}_T$, a measure is performed to compute a set of target statistics $\mathbb{D}_T$. Starting from an initial network configuration $\mathbb{M}_I$, associated with the computed statistics data $\mathbb{D}_I$, an energy E is defined as the squared difference between the target and computed statistics, i.e.,

$$E = |\mathbb{D}_I - \mathbb{D}_T|^2. \tag{4}$$

The initial configuration is subsequently evolved (via small random perturbations) to minimize the energy (4) by allowing energy-increasing configurations in the early stages and only accept energy-decreasing configurations towards the end. This procedure is schematically illustrated in Fig. 3.

We now describe the key steps in the network reconstruction procedure in detail. The first step in the reconstruction is to build a topologically feasible initial network configuration that captures a subset of the prescribed statistics, i.e., the node number density c_0. This is achieved by placing (either randomly or in an ordered manner) a fixed number of nodes N in the simulation box of volume V and requiring that $c_0 = N/V$. Then the distribution of valence number $\mathbf{n}$ is realized by randomly connecting neighboring nodes (i.e., those with a separation distance within a prescribed value R_f) so that the reconstructed valence distribution converges to the target distribution. We denote this initial network by $\mathbb{M}_I$.

Next, the fiber length distribution $\mathbf{L}$ and orientation distribution Ω are realized by randomly perturbing the initial configuration. This is achieved by randomly selecting a node in the old network configuration $\mathbb{M}_{\text{old}}$ and applying a random displacement to this node (see Fig. 4). This random perturbation results in a new configuration $\mathbb{M}_{\text{new}}$, in which both the length and orientation of the fibers connected to the displaced nodes (highlighted with red color or dark gray in the print version in Fig. 4) are changed. The corresponding network statistics $\mathbb{D}_{\text{new}}$ are then computed. We note that in computing $\mathbb{D}_{\text{new}}$, there is no need to directly applying the time-consuming mapping $\mathbb{D}_{\text{new}} = \mathscr{F}[\mathbb{M}_{\text{new}}]$, as the difference between $\mathbb{D}_{\text{new}}$ and $\mathbb{D}_{\text{old}}$ is entirely due to the local perturbation of a node. Therefore, only the changes of lengths and relative orientation of the perturbed fibers are computed and the corresponding

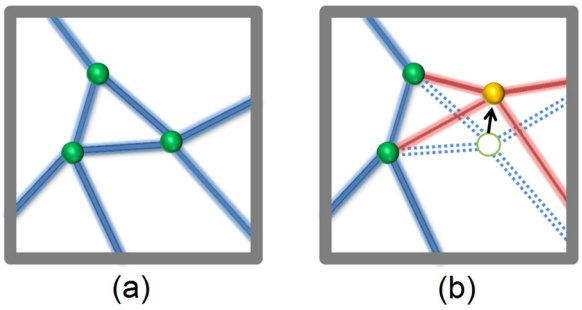

FIG. 4. Randomly displacing an arbitrary node in the network to generate a new configuration (b) from an old configuration (a). The fibers affected by this perturbation are highlighted using red color (or dark gray in the print version).

statistics in $\mathbb{D}_{\text{old}}$ are updated in order to quickly obtain $\mathbb{D}_{\text{new}}$. Then energies E_{old} and E_{new} respectively associated with the old and new configurations are then computed according to Eq. (4). In addition, we use periodic boundary conditions for reconstruction simulations.

In the simulated annealing approach, the new configuration is accepted with the following probability:

$$p_{\text{acc}}(\text{old} \to \text{new}) = \min\left[1, \exp\left(\frac{E_{\text{old}} - E_{\text{new}}}{T}\right)\right], \quad (5)$$

where T is a virtual temperature that is chosen to be initially high and slowly decreases according to the annealing schedule $T(n) = 0.95^n T_0$ (n is the annealing stage and T_0 is the initial temperature). The procedure is terminated when a prescribed tolerance on the energy is achieved (e.g., $E < 10^{-7}$). The final network configuration $\mathbb{M}_F$ is considered as a realization of $\mathbb{M}_T$, possessing statistics $\mathbb{D}_F$ that is virtually identical to the target corresponding to the target $\mathbb{D}_T$.

B. Handling heterogeneous collagen networks

For spatially heterogeneous networks, at least one type of the statistics in the data set $\mathbb{D}$ varies at different spatial locations in the system, i.e., the statistics are position dependent $\mathbb{D}(\mathbf{x})$. For such a system, the reconstruction domain is prepartitioned into regular subdomains. Each subdomain is sufficiently small such that the statistics associated with the network within each subdomain can be considered invariant. Accordingly, the reconstruction is formulated such that an initial network configuration is evolved to match the prescribed statistics in each subdomain. Thus, the energy of a spatially heterogeneous network is defined as

$$E = \sum_i \left|\mathbb{D}^{(i)} - \mathbb{D}_T^{(i)}\right|^2, \quad (6)$$

where $\mathbb{D}^{(i)}$ is statistics of ith subdomain in the simulated network and $\mathbb{D}_T^{(i)}$ is the corresponding target statistics.

The general reconstruction procedure described in Sec. II A can be readily generalized to handle heterogeneous networks. In particular, as the reconstruction domain is partitioned into subdomains, the random node displacement might lead to the transition of a node and the associated fibers from one subdomain to another. Here we consider a specific fiber belongs to subdomain i if the midpoint of this fiber is in subdomain i. Therefore, once a trial nodal displacement is made, the new length and orientation of fibers connected to the perturbed node are computed. In addition, the new midpoint position of each perturbed fiber is also obtained. If the perturbed fiber remains in the original subdomain before the perturbation, the "energy" associated with this subdomain is updated as in the homogeneous network case. However, if the perturbed fiber undergoes a transition from one subdomain to a neighbor subdomain, its contribution to the original subdomain is subtracted from the associated statistics and its contribution to the new subdomain is added to the associated statistics. Accordingly, the energies of both subdomains are updated to compute E_{new}, based on which the acceptance rate for the nodal displacement is computed.

In subsequent discussion, we will mainly consider heterogeneous networks with varying fiber orientation with respect to the z axis, while the fiber length distribution and valence distributions are spatial invariant. Such network systems are most relevant to the *in vitro* heterogeneous ECM reported in Ref. [83].

III. MICROMECHANICAL MODEL OF COLLAGEN NETWORK

In this section we briefly describe our micromechanical model for force analysis in cellularized ECM. The ensuing discussion follows closely to that in Ref. [21], to which the interested readers are referred to for more details.

Specifically we employ a nonlinear elastic model recently developed by Steinwachs *et al.* to characterize the stretching and compression of a collagen fiber [98]. In particular, upon stretching, a fiber first enters a linear elastic regime, which is followed by a strong strain-hardening regime once the elongation is larger than a prescribed threshold. Upon compression, we consider the fiber immediately buckles and thus, possesses a much smaller compression modulus. The elongation stiffness k of the fiber is thus given by

$$k = \begin{cases} \rho EA, & \lambda < 0, \\ EA, & 0 < \lambda < \lambda_s, \\ EA\exp[(\lambda - \lambda_s)/\lambda_0], & \lambda > \lambda_s, \end{cases} \quad (7)$$

where E and A are, respectively, the Young's modulus and cross-sectional area of the fiber bundle, and we use $EA = 8 \times 10^{-7} N$ [45]; $\lambda = \delta\ell/\ell$ is elongation strain, and $\lambda_s = 0.02$ and $\lambda_0 = 0.05$ are parameters for the strain-hardening model [98]; $\rho \in [0,1)$ describes the effects of buckling [74].

We model an embedded polarized cell as an ellipsoid with semiaxis $R_a = R_b < R_c$ respectively along the x, y, and z axis, centered at a prescribed location in the network. This simple shape is our first attempt to model a migrating cell which typically develops a polarized morphology [66]. The contraction of the cell pulls the nodes residing within a cone region defined by the polar angle θ in the cell towards the cell center, which is modeled by an affine transformation with a contraction ratio γ (see Fig. 5). In the subsequent simulations we use $\theta = \pi/2$ and $\gamma = 0.93$.

After cell contraction, a force-based relaxation method is employed to obtain the force-equilibrium network

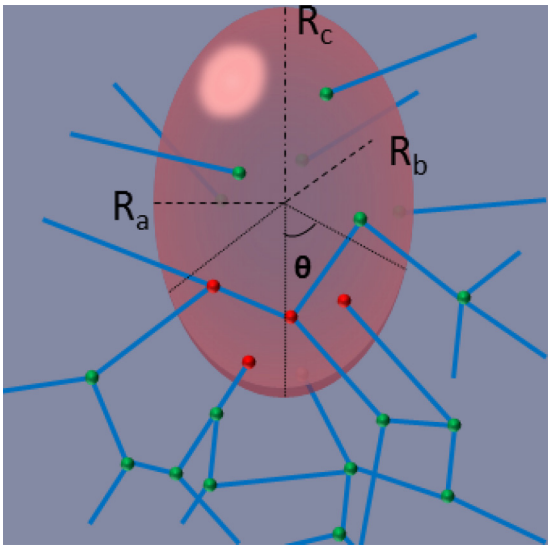

FIG. 5. Schematic illustration of the polarized contraction of an ellipsoidal cell embedded in the collagen network. The nodes within a cone region defined by the polar angle θ are pulled towards the cell center by an affine transformation.

configuration and resolve the forces on each fiber. Specifically, at each iteration, a node i is displaced along the direction of the net force on this node, with the magnitude of the displacement proportional to the magnitude of the force $\mathbf{F}^i$, i.e.,

$$\delta_i = \mu |\mathbf{F}^i|, \tag{8}$$

where δ_i is the magnitude of the displacement and μ is an effective mobility parameter. The upper bound of μ is chosen such that the maximal individual displacement is $\sim 1/100$ of the average fiber length. Once the positions of all nodes are updated, the new net force of each node is computed, which determines the nodal displacement. This process is repeated until the maximal net force on a node is smaller than a prescribed tolerance (e.g., $<10^{-10}$ N).

IV. RECONSTRUCTION RESULTS

A. Homogeneous collagen networks with randomly oriented fibers

We first employ the procedure described in Sec. II A to reconstruct realizations of a homogeneous collagen network with randomly oriented fibers. Specifically, the collagen gel is prepared with a collagen concentration of 1 mg/mL and a gelation temperature of 30 °C. The critical network statistics used for the reconstruction, including the valence distribution **n** and the fiber length distribution **L**, are extracted from a 3D bond-node model constructed from the 3D confocal microscopy image of the network and shown in Fig. 6. The average valence number is $n^* = 3.38$; and the average fiber length is $\ell^* = 1.96$ μm. The orientation of the fiber is quantified via absolute value of direction cosine of the angle ϕ between a fiber and the z axis. Then the overall fiber orientation is characterized by

$$\Omega^* = \frac{1}{N_f} \sum_i \cos\phi_i, \tag{9}$$

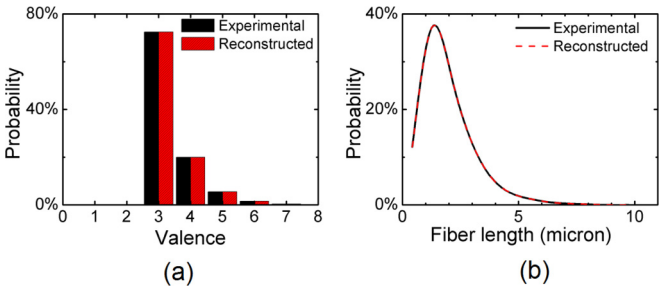

FIG. 6. Target and simulated network statistics including the valence number distribution (a) and the fiber length distribution (b) for a homogeneous network with randomly oriented fibers.

where N_f is the total number of fibers. In this collagen gel with randomly oriented fibers, we have $\Omega^* = 0.5$. In addition, the reconstruction domain is a cubic box with a linear size of 45 μm and the total number of nodes in the box is 40 000.

Taking the aforementioned network statistics as a target data set, the simulated annealing procedure described in Sec. II A is employed to generalize realizations of the network with virtually identical statistics. In particular, we employ a power-law cooling schedule, i.e., $T(n) = T_0 0.95^n$, which is also shown in Fig. 7(a), as a function of the reconstruction stages n. The evolution of the average energy E of each stage is shown in Fig. 7(b). It can been seen that after the initial fast decay, the energy gradually decreases to zero, indicating the convergence of reconstruction. We note that within each reconstruction stage, a certain number of energy-increasing configurations are accepted. However, the average energy of a particular stage is a monotonic decreasing function of the number of stages.

Figure 8 shows a 3D visualization of the reconstructed network that is statistically identical to the target collagen network as obtained using 3D confocal microscopy imaging. In addition, the distribution of valence number and fiber length of the reconstructed system are quantitatively compared to the corresponding target data and are shown in Fig. 6. It can be seen that the statistics of the reconstructed network are virtually indistinguishable from the corresponding target data. Indeed, the final energy E_f quantifying the difference between the data sets is smaller than $\sim 10^{-9}$. This clearly indicates the validity and efficiency of our procedure.

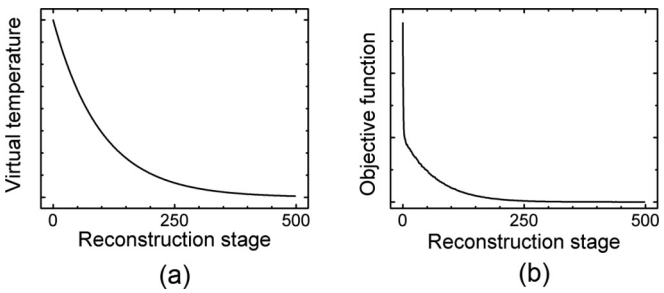

FIG. 7. (a) Power-law cooling schedule used for the reconstruction. (b) Evolution of the average energy of each stage during the reconstruction.

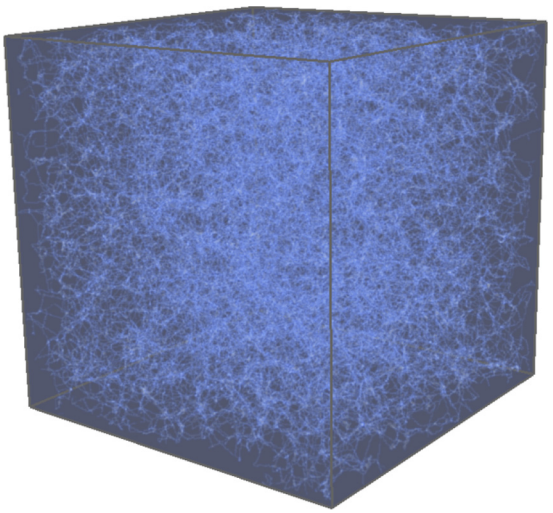

FIG. 8. 3D visualization of the reconstructed homogeneous network with randomly oriented fibers that is statistically identical to the target collagen network as obtained using 3D confocal microscopy imaging.

B. Homogeneous collagen networks with prealigned fibers

We now apply the procedure to generate realizations of homogeneous network with prealigned fibers. We consider this network possesses the same node density, distribution of valence number, and distribution of fiber length as in Sec. IV A. However, the fiber orientation is now characterized by the average cosine value $\Omega^* = 1$. This corresponds to the ideal case that all fibers perfectly align with the z axis in the system. In the actual network, due to the geometrical and topological constraints, it is not possible to achieve such a perfect configuration. Nonetheless, it is interesting to see what is the highest Ω^* that can be achieved in a network by setting the target value to be unity. The same annealing parameters in Sec. IV A are used here.

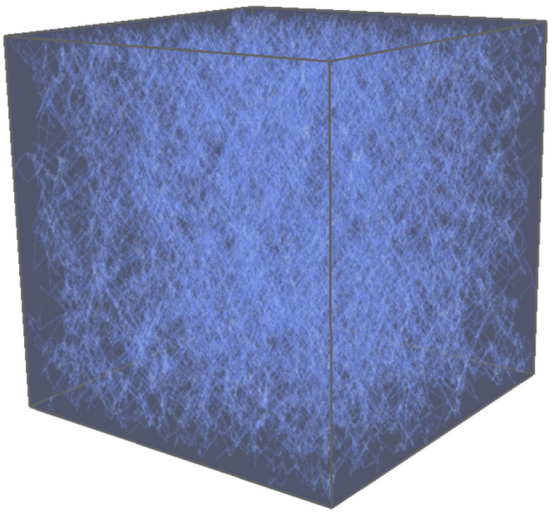

FIG. 9. 3D visualization of the reconstructed homogeneous network with fibers aligned with the z axis.

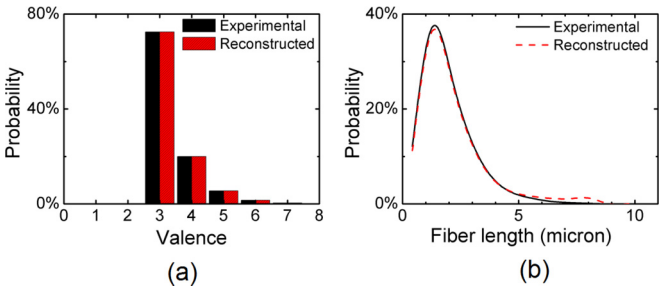

FIG. 10. Target and simulated network statistics including the valence number distribution (a) and the fiber length distribution (b) for a homogeneous network with prealigned fibers.

Figure 9 shows a 3D visualization of the reconstructed homogenous network. It can be clearly seen that the fibers tend to align with the z axis to maximize the Ω^* value. The final reconstructed network possesses a $\Omega^* = 0.86$. As we will see in Sec. V, the alignment of the fibers can significantly enhance the propagation of the active force generated by a contractile cell embedded in the collagen network.

Figure 10 shows the quantitative comparison of the target and reconstructed network statistics including the distribution of valence number and fiber length. It can be seen that the reconstructed valence distribution matches very well with the target distribution. However, there are some small discrepancies between the reconstructed fiber length distribution and the target distribution (derived originally from networks with randomly oriented fibers). In particular, the reconstructed network possesses a slightly larger number of long fibers. We believe these additional long fibers are geometrically necessary to achieve the high degree of alignment of the fibers.

C. Heterogeneous collagen networks with continuous variation of fiber orientation

In this section we consider a heterogeneous collagen network with continuous variation of fiber orientation along the z axis. Such a network can be engineered [83] to systematically investigate contact guidance effects during cancer cell invasion. Specifically, we employ a cuboidal reconstruction domain with a linear dimension of 45 μm, which contains 40 000 nodes. The domain is partitioned into 11 equal-sized regions along the z direction. As one travels along the z direction from the bottom region to the top region, the fiber orientations vary from that perpendicular to the z axis to that parallel to the z axis. The average orientation cosine value $\Omega^*(z)$ as a function of z is shown in Fig. 11. The other network statics including the distribution of nodal valence number of fiber length are the same as in Sec. IV A. The same annealing parameters in Sec. IV A are used here.

Figure 11 shows a 3D visualization of the reconstructed heterogeneous network. The continuous variation of the fiber orientations from the bottom to the top of the simulation box can be clearly seen. Figure 12 shows the quantitative comparison of the target and reconstructed $\Omega^*(z)$. Similar to the case in Sec. IV B, the large Ω^* values (i.e., those close to unity) are not exactly realizable due to the geometrical and topological constraints. For example, it is not possible that

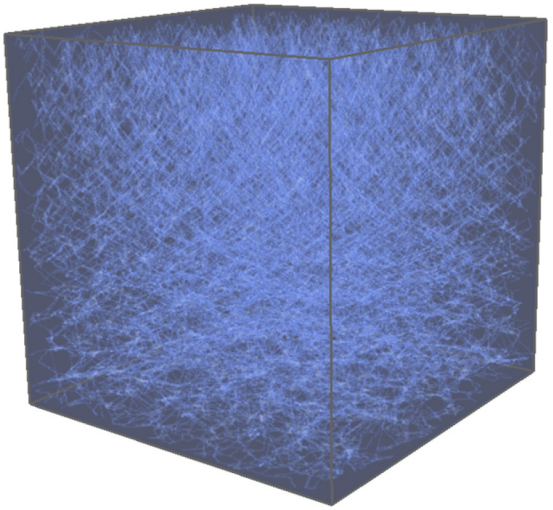

FIG. 11. 3D visualization of the reconstructed heterogeneous collagen network with continuous variation of fiber orientation along the z axis.

all of the fibers in the network are perfectly aligned with the z axis while still maintaining a uniform distribution of the nodes. Nonetheless, the majority of the fibers in the top regions of the reconstructed network tend to align with the z axis as required by the target Ω^*. Figure 13 shows the network statistics including the distribution of valence number and fiber length. Again, it can be seen that the reconstructed valence distribution matches very well with the target distribution, while the reconstructed network possesses a slightly larger number of long fibers, which are geometrically necessary to achieve the high degree of alignment of the fibers.

D. Highly heterogeneous ECM containing collagen and Matrigel

In this section we consider a highly heterogeneous network system that mimics the heterogeneous ECM experimentally constructed in Ref. [83]. In our simulation, the network contains a region with prealigned fibers mimicking a collagen gel with oriented fibers and a region with randomly oriented fibers

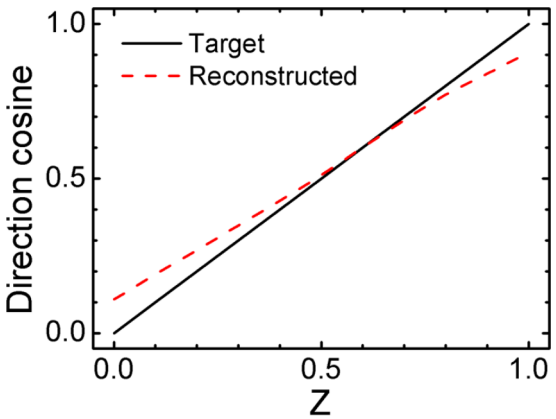

FIG. 12. The target and simulated $\Omega^*(z)$ (i.e., the average cosine value of the angle between the fibers and z axis) as a function of z position (normalized with respect to the box length) in the network.

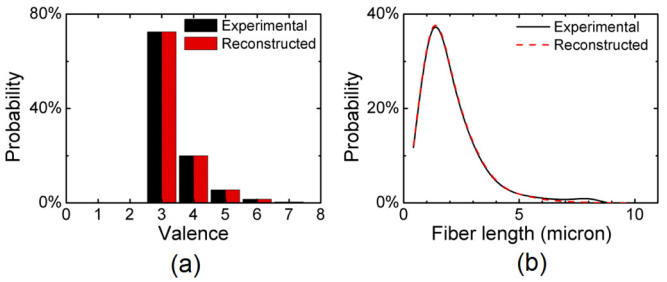

FIG. 13. Target and simulated network statistics including the valence number distribution (a) and the fiber length distribution (b) for a heterogeneous network with continuously varying fiber orientations.

mimicking the Matrigel region. The reconstruction domain is a cubic box with a linear size of 45 μm and the total number of nodes in the box is 40 000. The upper region which occupies 73% of the volume contains collagen fibers aligned with the z axis. This is achieved by imposing $\Omega^* = 1$, as in Sec. IV B. The lower region which occupies 27% of the volume contains randomly oriented fibers, characterized by $\Omega^* = 0.4$. The other network statics including the distribution of nodal valence number of fiber length are considered the same for both regions and the data in Sec. IV A are used here. The same annealing parameters in Sec. IV A are used here.

Figure 14 shows a 3D visualization of the reconstructed heterogeneous network. The contrast between the region with aligned fibers and the region with randomly oriented fibers can be clearly seen. Figure 15 shows the quantitative comparison of the target and reconstructed $\Omega^*(z)$ values, which again shows the expected discrepancies for the region with oriented fibers. Figure 16 shows the network statistics including the distribution of valence number and fiber length. We note that these reconstruction studies not only allow us to generate realizations of ECM networks with desirable microstructural properties quantified by $\mathbb{D}$, but also enable us to explore the theoretical limits associated with specific network statistics such as Ω^*.

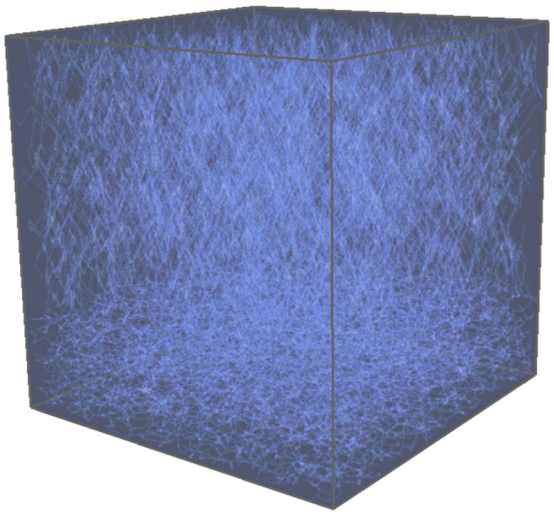

FIG. 14. 3D visualization of the reconstructed heterogeneous collagen network with a collagen region composed of aligned fibers and a Matrigel region composed of randomly oriented fibers.

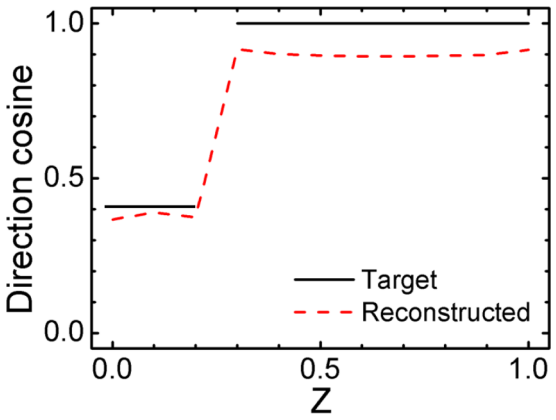

FIG. 15. The target and simulated $\Omega^*(z)$ (i.e., the average cosine value of the angle between the fibers and z axis) as a function of z position (normalized with respect to the box length) in the network.

V. MICROMECHANICAL ANALYSIS OF CANCER CELL INTRAVASATION

We now investigate the effects of the ECM microstructure on the propagation of the active forces generated by a polarized contractile cell embedded in the system. Specifically, an ellipsoidal cell with semiaxes $a = b = 6.84$ μm and $c = 10.26$ μm is embedded in the center of the simulated network, whose c axis is aligned with the z axis. An affine contraction toward the cell center is applied to the nodes included in the lower semiellipsoid region with a contraction ratio $\gamma = 0.93$ (see Sec. III for details). The force-based relaxation method is subsequently employed to find force equilibrium network configuration as described in Sec. III. The force network is visualized by coloring the fibers carrying a force larger than 5.0×10^{-7} N, which is about 2.5% of the largest force in the network.

Figure 17 shows the propagation of active forces generated by a polarized contractile cell in a homogeneous network with randomly oriented fibers [Fig. 17(a)], a homogeneous network with prealigned fibers [Fig. 17(b)], and a heterogeneous network with continuously varying fiber orientations along the z axis [Fig. 17(c)] reconstructed in Sec. IV C. In particular, the fibers originally aligned perpendicular to the z axis are gradually aligned along the z axis as one travels from the bottom to the top of the heterogeneous network. It can be clearly seen that oriented fibers can significantly enhance the propagation

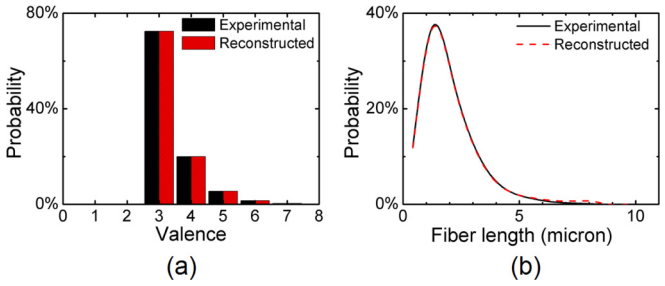

FIG. 16. Target and simulated network statistics including the valence number distribution (a) and the fiber length distribution (b) for the binary heterogeneous network.

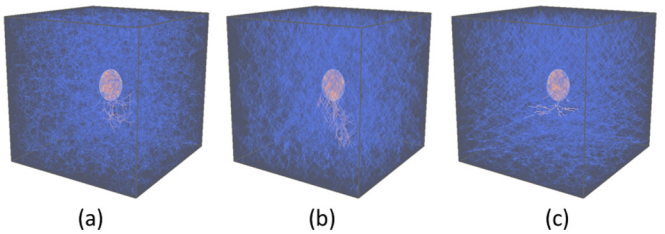

FIG. 17. Propagation of active forces generated by a polarized contractile cell in a homogeneous network with randomly oriented fibers (a), a homogeneous network with prealigned fibers (b), and a heterogeneous network with continuously varying fiber orientations along the z axis (c). The fibers carrying large forces ($>5.0 \times 10^{-7}$ N) are highlighted using red color (dark gray in the print version).

of active forces. In particular, in the network with randomly oriented fibers, the force chains (indicated by the highlighted fibers carrying large forces) only extend isotropically to a small region (with a linear dimension $\sim$5 μm) surrounding the contracting surface of the cell. On the other hand, in the network with prealigned fibers, the force chains can extend through the entire system and reach the boundary of the simulation box. In addition, in this case, the force propagation is highly directional along the z axis with a linear extent of at least 20 μm. We note that the alignment of the fibers can significantly diminish the reduction of the forces when passing through two successive fibers, and thus lead to the enhanced force propagation. In the case of the heterogeneous network, the continuously varying fiber orientations can effectively redirect the force chains. Specifically, close to the cell surface, the stress fibers tend to align with the z axis, which is due to the direction of the contraction. As the force chains propagate, they quickly bend over to be perpendicular to the z axis. This leads to a relatively small penetration depth in the z direction, with $\sim$5 μm. However, the linear extent of the force chains perpendicular to the z axis is $\sim$10 μm.

Figure 18 shows the propagation of active forces generated by a polarized contractile cell in a highly heterogeneous ECM composed a collagen region (upper) with prealigned fibers and a Matrigel region (lower) with randomly oriented fibers, mimicking the *in vitro* heterogeneous microenvironment studied in Ref. [83]. It can be clearly seen that the highly directional force chains composed of the fibers carrying large forces ($>5.0 \times 10^{-7}$ N) (highlighted using red color or dark gray in the print version) expand through the entire oriented collagen region and deeply penetrate into the Matrigel region. With the Matrigel, due to the initial random fiber orientations, the force propagation becomes more isotropic, compared to that in the oriented collagen region.

In addition, we also investigate the remodel of the Matrigel by the active cellular forces, which is quantified by the changes in the fiber orientations before and after the cell contraction. Specifically, the angles between a high-stress fiber in the Matrigel region and the z axis before and after cell contraction are computed and shown in Fig. 19, in which the size of the circle indicates the magnitude of the forces on the fiber. It can be seen that a large number of Matrigel fibers, which carry relative large forces, are reoriented along the z direction by the active cellular forces. We believe that these reoriented

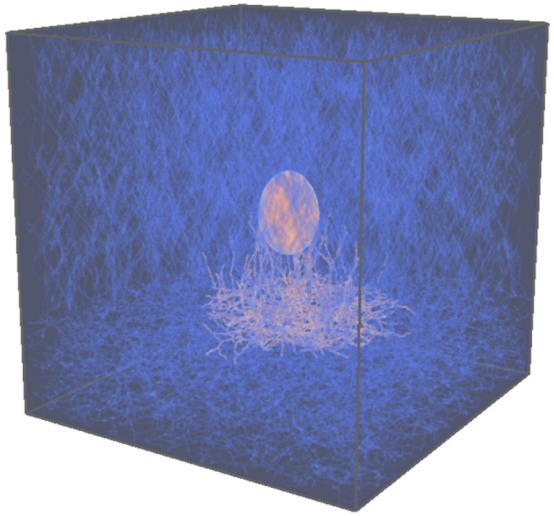

FIG. 18. Propagation of active forces generated by a polarized contractile cell in a highly heterogeneous ECM composed a collagen region (upper) with prealigned fibers and a Matrigel region (lower) with randomly oriented fibers. The fibers carrying large forces ($>5.0 \times 10^{-7}$ N) are highlighted using red color (dark gray in the print version).

high-stress fibers can provide strong contact guidance for the migrating MDA-MB-231 cells that penetrate into the Matrigel region, which further facilitate their invasion. This could provide a possible mechanism for the observed enhanced tumor cell intravasation by oriented collagen [83].

Finally, we investigate the effects of collectiveness during tumor cell invasion. In particular, we embed a small group of (e.g., four) polarized ellipsoidal cells in the collagen (upper) part of the ECM. The positions of the cell centers are given by (0, 0, 0) μm, (0, 7.5, 5) μm, (6.5, -3.75, 5) μm, and (-6.5, -3.75, 5) μm with respect to the center of the simulation box. The longest semiaxis of each cell is aligned with the z axis. All four cells contract together with the same contraction ratio as in the single cell case. This particular configuration

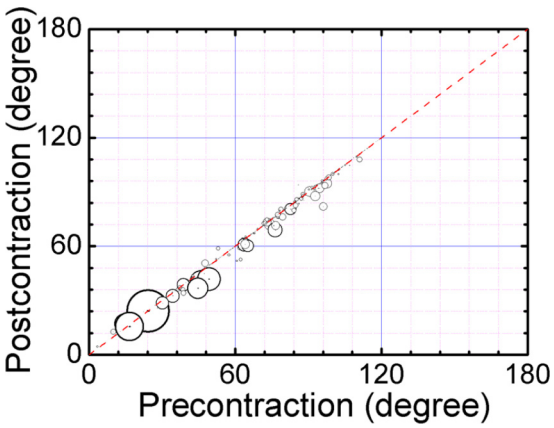

FIG. 19. Comparison of the angle between a fiber in the Matrigel and the z axis before and after the contraction of the cell. The size of the circle indicates the force magnitude in the fiber. Reorientation of the fibers carrying relatively large forces along the z axis can be observed.

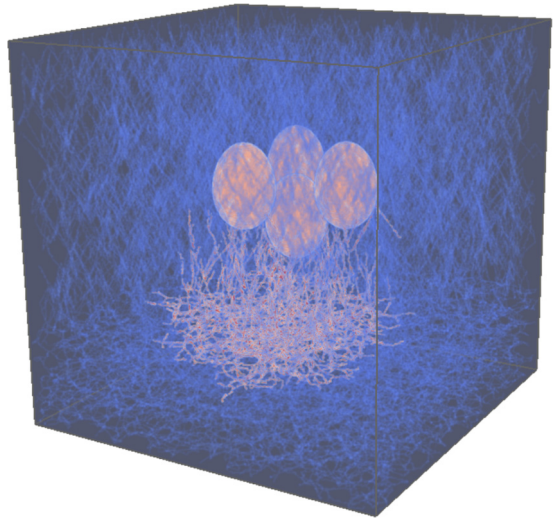

FIG. 20. Propagation of active forces generated by a group of polarized contractile cells mimicking a tumor invasion front in a highly heterogeneous ECM composed a collagen region (upper) with prealigned fibers and a Matrigel region (lower) with randomly oriented fibers. The fibers carrying large forces ($>5.0 \times 10^{-7}$ N) are highlighted using red color (dark gray in the print version).

is chosen to mimic the invasion front of breast cancer cells observed *in vitro*. Figure 20 shows the propagation of active forces generated by the small cell group. Figure 21 shows the reorientation of the fibers in the Matrigel (lower) part of heterogenous ECM. Similar to the single cell case, the deep penetration of force chains into the Matrigel region can be clearly seen. In addition, a stronger reorientation effect has been observed from Fig. 21, as indicated by the increasing number of large circles in the lower right region of the plot. This result implies that collective cell contraction and migration can further promote prealignment of Matrigel fibers and thus facilitate the intravasation.

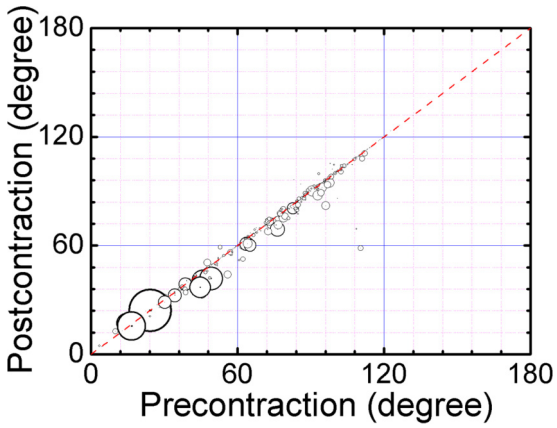

FIG. 21. Comparison of the angle between a fiber in the Matrigel and the z axis before and after the collective contraction of the group of tumor cells. The size of the circle indicates the force magnitude in the fiber. Reorientation of the fibers carrying relatively large forces along the z axis can be observed.

VI. CONCLUSIONS AND DISCUSSION

In this paper we devised a procedure for generating realizations of highly heterogeneous 3D collagen networks with prescribed microstructural statistics including the node density, valence number distribution, fiber length distribution, as well as fiber orientations via stochastic optimization. Specifically, the realization (reconstruction) is formulated as an optimization problem in which the objective function, defined on the space of the network configurations, is the squared difference between a set of target microstructural statistics and the corresponding statistics for the simulated network. Simulated annealing is employed to solve the optimization problem by evolving an initial network via random perturbations to search the network configuration space and eventually generate a realization compatible with the specified target statistics. We have employed this procedure to generate of a variety of ECM systems, including homogeneous networks with randomly oriented fibers, homogeneous networks with aligned fibers, heterogeneous networks with a continuous variation of fiber orientation along a prescribed direction, as well as a binary system containing a collagen region with aligned fibers and a dense Matrigel region with randomly oriented fibers.

The realizations of heterogeneous networks with distinct structural features have allowed us to systematically investigate the effects of network microstructure on the propagation of active forces in the simulated networks. Specifically, the polarized contraction of an embedded ellipsoidal cell is applied and the distribution of the resulting forces is analyzed by considering a nonlinear fiber model incorporating strain hardening upon large stretching and buckling upon compression. Our analysis shows that oriented fibers can significantly enhance long-range force transmission in the network. Moreover, in the collagen-Matrigel system, the forces generated by a polarized cell in collagen can penetrate deeply into the Matrigel region. The stressed Matrigel fibers could provide contact guidance for the migrating cells, and thus enhance their penetration into Matrigel.

We note that the current analysis focuses on static contraction of a single model cell. The realizations of the distinct network configurations also allow us to systematically investigate the effects of ECM microstructure on dynamic cell-ECM interactions as well as the resulting collective multicell behaviors. In such cases, a cell not only generates active forces by pulling the ECM fibers but also senses and responds to the forces exerted via the fibers. Such investigations will be reported in our future publications.

ACKNOWLEDGMENTS

H.N. and Y.J. thank Arizona State University for the generous start-up funds. This work is partially supported by the National Science Foundation of China under Grants No. 11474345, No. 11674043, and No. 11574382.

[1] H. Lodish, A. Berk, S. L. Zipursky, P. Matsudaira, D. Baltimore, and J. Darnell, *Molecular Cell Biology*, 4th ed. (W. H. Freeman, New York, 2000), Chap. 22.

[2] A. J. Ridley, M. A. Schwartz, K. Burridge, R. A. Firtel, M. H. Ginsberg, G. Borisy, J. T. Parsons, and A. R. Horwitz, Cell migration: Integrating signals from front to back, Science **302**, 1704 (2003).

[3] J. D. Humphrey, E. R. Dufresne, and M. A. Schwartz, Mechanotransduction and extracellular matrix homeostasis, Nat. Rev. Mol. Cell Biol. **15**, 802 (2014).

[4] C. Bonnans, J. Chou, and Z. Werb, Remodelling the extracellular matrix in development and disease, Nat. Rev. Mol. Cell Biol. **15**, 786 (2014).

[5] R. J. Pelham, Y. L. Wang, and Y. Wang, Cell locomotion and focal adhesions are regulated by substrate flexibility, Proc. Natl. Acad. Sci. USA **94**, 13661 (1997).

[6] T. Yeung, P. C. Georges, L. A. Flanagan, B. Marg, M. Ortiz, M. Funaki, N. Zahir, W. Ming, V. Weaver, and P. A. Janmey, Effects of substrate stiffness on cell morphology, cytoskeletal structure, and adhesion, Cytoskeleton **60**, 24 (2005).

[7] A. J. Engler, S. Sen, H. L. Sweeney, and D. E. Discher, Matrix elasticity directs stem cell lineage specification, Cell **126**, 677 (2006).

[8] K. R. Levental, H. Yu, L. Kass, J. N. Lakins, M. Egeblad, J. T. Erler, S. F. T. Fong, K. Csiszar, A. Giaccia, W. Weninger, M. Yamauchi, D. L. Gasser, and V. M. Weaver, Matrix crosslinking forces tumor progression by enhancing integrin signaling, Cell **139**, 891 (2009).

[9] R. W. Tilghman, C. R. Cowan, J. D. Mih, Y. Koryakina, D. Gioeli, J. K. Slack-Davis, B. R. Blackman, D. J. Tschumperlin, and J. T. Parsons, Matrix rigidity regulates cancer cell growth and cellular phenotype, PLoS One **5**, e12905 (2010).

[10] E. Hadjipanayi, V. Mudera, and R. A. Brown, Guiding cell migration in 3D: A collagen matrix with graded directional stiffness, Cell Motil. Cytoskeleton **66**, 121 (2009).

[11] S. Guido and R. T. Tranquillo, A methodology for the systematic and quantitative study of cell contact guidance in oriented collagen gels. Correlation of fibroblast orientation and gel birefringence, J. Cell Sci. **105**, 317 (1993).

[12] P. P. Provenzano, D. R. Inman, K. W. Eliceiri, S. M. Trier, and P. J. Keely, Contact guidance mediated three-dimensional cell migration is regulated by Rho/ROCK-dependent matrix reorganization, Biophys. J. **95**, 5374 (2008).

[13] T. R. Cox and J. T. Erler, Remodeling and homeostasis of the extracellular matrix: Implications for fibrotic diseases and cancer, Dis. Model Mech. **4**, 165 (2011).

[14] J. Kim, J. Feng, C. A. R. Jones, X. Mao, L. M. Sander, H. Levine, and B. Sun, Stress-induced plasticity of dynamic collagen networks, Nat. Commun. **8**, 842 (2017).

[15] H. Wang, A. S. Abhilash, C. S. Chen, R. G. Wells, and V. B. Shenoy, Long-range force transmission in fibrous matrices enabled by tension-driven alignment of fibers, Biophys. J. **107**, 2592 (2014).

[16] R. K. Sawhney and J. Howard, Slow local movements of collagen fibers by fibroblasts drive the rapid global self-organization of collagen gels, J. Cell Biol. **157**, 1083 (2002).

[17] C. A. R. Jones, M. Cibula, J. Feng, E. A. Krnacik, D. H. McIntyre, H. Levine, and B. Sun, Micromechanics of cellularized biopolymer networks, Proc. Natl. Acad. Sci. USA **112**, E5117 (2015).

[18] Y. L. Han, P. Ronceray, G. Xu, A. Malandrino, R. Kamm, M. Lenz, C. P. Broedersz, and M. Guo, Cell contraction induces long-ranged stress stiffening in the extracellular matrix, arXiv:1709.00793.

[19] X. Ma, M. E. Schickel, M. D. Stevenson, A. L. Sarang-Sieminski, K. J. Gooch, S. N. Ghadiali, and R. T. Hart, Fibers in the extracellular matrix enable long-range stress transmission between cells, Biophys. J. **104**, 1410 (2013).

[20] Q. Shi, R. P. Ghosh, H. Engelke, C. H. Rycroft, L. Cassereau, J. A. Sethian, V. M. Weaver, and J. T. Liphardt, Rapid disorganization of mechanically interacting systems of mammary acini, Proc. Natl. Acad. Sci. USA **111**, 658 (2013).

[21] L. Liang, C. Jones, S. Chen, B. Sun, and Y. Jiao, Heterogeneous force network in 3D cellularized collagen networks, Phys. Biol. **13**, 066001 (2016)

[22] P. Ronceray, C. P. Broedersz, and M. Lenz, Fiber networks amplify active stress, Proc. Natl. Acad. Sci. USA **113**, 2827 (2016).

[23] T. Lecuit, P.-F. Lenne, and E. Munro, Force generation, transmission, and integration during cell and tissue morphogenesis, Annu. Rev. Cell Dev. Biol. **27**, 157 (2011).

[24] R. Fernandez-Gonzalez, S. de M. Simoes, J. C. Röper, S. Eaton, and J. A. Zallen, Myosin II dynamics are regulated by tension in intercalating cells, Dev. Cell **17**, 736 (2009).

[25] G. Totsukawa, Y. Wu, Y. Sasaki, D. J. Hartshorne, Y. Yamakita, S. Yamashiro, and F. Matsumura, Distinct roles of MLCK and ROCK in the regulation of membrane protrusions and focal adhesion dynamics during cell migration of fibroblasts, J. Cell Biol. **164**, 427 (2004).

[26] K. Jakab, A. Neagu, V. Mironov, R. R. Markwald, and G. Forgacs, Engineering biological structures of prescribed shape using self-assembling multicellular systems, Proc. Natl. Acad. Sci. USA **101**, 2864 (2004).

[27] A. D. Doyle, N. Carvajal, A. Jin, K. Matsumoto, and K. M. Yamada, Local 3D matrix microenvironment regulates cell migration through spatiotemporal dynamics of contractility-dependent adhesions, Nat. Commun. **6**, 8720 (2015).

[28] F. Beroz, L. M. Jawerth, S. Munster, D. A. Weitz, C. P. Broedersz, and N. S. Wingreen, Physical limits to biomechanical sensing in disordered fibre networks, Nat. Commun. **8**, 16096 (2017).

[29] A. A. Alobaidi, Y. Xu, S. Chen, Y. Jiao, and B. Sun, Probing cooperative force generation in collective cancer invasion, Phys. Biol. **14**, 045005 (2017).

[30] P. Friedl and D. Gilmour, Collective cell migration in morphogenesis, regeneration and cancer, Nat. Rev. Mol. Cell Biol. **10**, 445 (2009).

[31] M. A. Wozniak and C. S. Chen, Mechanotransduction in development: A growing role for contractility, Nat. Rev. Mol. Cell Biol. **10**, 34 (2009).

[32] D. E. Jaalouk and J. Lammerding, Mechanotransduction gone awry, Nat. Rev. Mol. Cell Biol. **10**, 63 (2009).

[33] M. E. Lukashev and Z. Werb, ECM signalling: Orchestrating cell behaviour and misbehaviour, Trend. Cell Biol. **8**, 437 (1998).

[34] R. Sunyer, V. Conte, J. Escribano, A. Elosegui-Artola, A. Labernadie, L. Valon, D. Navajas, J. M. Garcia-Aznar, J. J. Munoz, P. Roca-Cusachs, and X. Trepat, Collective cell durotaxis emerges from long-range intercellular force transmission, Science **353**, 1157 (2016).

[35] N. R. Lang, S. Munster, C. Metzner, P. Krauss, S. Schurmann, J. Lange, K. E. Aifantis, O. Friedrich, and B. Fabry, Estimating the 3D pore size distribution of biopolymer networks from directionally biased data, Biophys. J. **105**, 1967 (2013).

[36] W. Mickel, S. Munster, L. M. Jawerth, D. A. Vader, D. A. Weitz, A. P. Sheppard, K. Mecke, B. Fabry, and G. E. Schruder-Turk, Robust pore size analysis of filamentous networks from three-dimensional confocal microscopy, Biophys. J. **95**, 6072 (2008).

[37] S. R. Gujarathi, C. L. Farrow, C. Glosser, L. Granlund, and P. M. Duxbury, *Ab initio* reconstruction of complex Euclidean networks in two dimensions, Phys. Rev. E **89**, 053311 (2014).

[38] F. J. O'Brien, B. A. Harley, M. A. Waller, I. V Yannas, L. J. Gibson, and P. J. Prendergast, The effect of pore size on permeability and cell attachment in collagen scaffolds for tissue engineering, Tech. Health Care **15**, 3 (2007).

[39] Y. L. Yang, S. Motte, and L. J. Kaufman, Pore size variable type I collagen gels and their interaction with glioma cells, Biomaterials **31**, 5678 (2010).

[40] A. G. Ogston, The spaces in a uniform random suspension of fibres, Trans. Faraday Soc. **54**, 1754 (1958).

[41] A. Takahashi, R. Kita, T. Shinozaki, K. Kubota, and M. Kaibara, Real space observation of three-dimensional network structure of hydrated fibrin gel, Colloid Polym. Sci. **281**, 832 (2003).

[42] Y. Jiao and S. Torquato, Quantitative characterization of the microstructure and transport properties of biopolymer networks, Phys. Biol. **9**, 036009 (2012).

[43] A. O. Brightman, B. P. Rajwa, J. E. Sturgis, M. E. McCallister, J. P. Robinson, and S. L. Voytik-Harbin, Time-lapse confocal reflection microscopy of collagen fibrillogenesis and extracellular matrix assembly in vitro, Biopolymers **54**, 222 (2000).

[44] J. Zhu and L. J. Kaufman, Collagen I self-assembly: Revealing the developing structures that generate turbidity, Biophys. J. **106**, 1822 (2014).

[45] S. B. Lindstrom, D. A. Vader, A. Kulachenko, and D. A. Weitz, Biopolymer network geometries: characterization, regeneration, and elastic properties, Phys. Rev. E **82**, 051905 (2010).

[46] C. A. R. Jones, L. Liang, D. Lin, Y. Jiao, and B. Sun, The spatial-temporal characteristics of type I collagen-based extracellular matrix, Soft Matter **10**, 8855 (2014).

[47] JR. K. Jain, Transport of molecules in the tumor interstitium: A review, Cancer Res. **47**, 3039 (1987).

[48] A. G. Ogston, B. N. Preston, and J. D. Wells, On the transport of compact particles through solutions of chain-polymers, Proc. R. Soc. London Ser. A **333**, 297 (1973).

[49] L. Johansson, C. Elvingson, and J. E. Lofroth, Diffusion and interaction in gels and solutions. 3. Theoretical results on the obstruction effect, Macromolecules **24**, 6024 (1991).

[50] L. Johansson and J. E. Lofroth, Diffusion and interaction in gels and solutions: I. Method, Colloid Interface Sci. **142**, 116 (1991).

[51] L. Johansson, U. Skantze, and J. E. Lofroth, Diffusion and interaction in gels and solutions. 2. Experimental results on the obstruction effect, Macromolecules **24**, 6019 (1991).

[52] L. Johansson and J. E. Lofroth, Diffusion and interaction in gels and solutions. 4. Hard sphere Brownian dynamics simulations, J. Phys. Chem. **98**, 7471 (1993).

[53] H. A. Leddy, M. A. Haider, and F. Guilak, Diffusional anisotropy in collagenous tissues: Fluorescence imaging of continuous point photobleaching, Biophys. J. **91**, 311 (2006).

[54] A. Erikson, H. N. Andersen, S. N. Naess, P. Sikorski, and C. D. L. Davies, Physical and chemical modifications of collagen gels: Impact on diffusion, Biopolymers **89**, 135 (2008).

[55] T. Stylianopoulos, B. Diop-Frimpong, L. L. Munn, and R. K. Jain, Diffusion anisotropy in collagen gels and tumors: The effect of fiber network orientation, Biophys. J. **99**, 3119 (2010).
[56] A. P. Chatterjee, Tracer diffusion in fibre networks: The impact of spatial fluctuations in the fibre distribution, J. Phys. Condens. Matter **23**, 375103 (2011).
[57] Y. L. Yang, L. M. Leone, and L. J. Kaufman, Elastic moduli of collagen gels can be predicted from two-dimensional confocal microscopy, Biophys. J. **97**, 2051 (2009).
[58] C. B. Raub, A. J. Putnam, B. J. Tromberg, and S. C. George, Predicting bulk mechanical properties of cellularized collagen gels using multiphoton microscopy, Acta Biomater. **6**, 4657 (2010).
[59] C. P. Broedersz, X. Mao, T. C. Lubensky, and F. C. Mackintosh, Criticality and isostaticity in fibre networks, Nat. Phys. **7**, 983 (2011).
[60] J. Feng, H. Levine, X. Mao, and L. M. Sander, Alignment and nonlinear elasticity in biopolymer gels, Phys. Rev. E **91**, 042710 (2015).
[61] H. Jiang, L. Jiang, J. D. Posner, and B. D. Vogt, Atomistic-based continuum constitutive relation for microtubules: Elastic modulus prediction, Comput. Mech. **42**, 607 (2008).
[62] J. Zhang, X. Zhao, Z. Suo, and H. Jiang, A finite element method for transient analysis of concurrent large deformation and mass transport in gels, J. Appl. Phys. **105**, 093522 (2009).
[63] A. M. Stein, D. A. Vader, D. A. Weitz, and L. M. Sander The micromechanics of three-dimensional collagen-I gels, Complexity **16**, 22 (2011).
[64] J. A. J. Van Der Rijt, K. O. Van Der Werf, M. L. Bennink, P. J. Dijkstra, and J. Feijen, Micromechanical testing of individual collagen fibrils, Macromol Biosci **6**, 697 (2006).
[65] M. Wyart, H. Liang, A. Kabla, and L. Mahadevan, Elasticity of Floppy and Stiff Random Networks, Phys. Rev. Lett. **101**, 215501 (2008).
[66] A. S. Abhilash, B. M. Baker, B. Trappmann, C. S. Chen, and V. B. Shenoy, Remodeling of fibrous extracellular matrices by contractile cells: Predictions from discrete fiber network simulations, Biophys. J. **107**, 1829 (2014).
[67] S. Motte and L. J. Kaufman, Strain stiffening in collagen I networks, Biopolymers **99**, 35 (2013).
[68] A. Guzman, M. J. Ziperstein, and L. J. Kaufman, The effect of fibrillar matrix architecture on tumor cell invasion of physically challenging environments, Biomaterials **35**, 6954 (2014).
[69] R. C. Arevalo, P. Kumar, J. S. Urbach, and D. L. Blair, Stress heterogeneities in sheared type-I collagen networks revealed by boundary stress microscopy, PloS One **10**, e0118021 (2015).
[70] C. Heussinger and E. Frey, Force distributions and force chains in random stiff fiber networks, Eur. Phys. J. E **24**, 47 (2007).
[71] D. A. Head, A. J. Levine, and F. C. MacKintosh, Mechanical response of semiflexible networks to localized perturbations, Phys. Rev. E **72**, 061914 (2005).
[72] Y. Shokef and S. A. Safran, Scaling Laws for the Response of Nonlinear Elastic Media with Implications for Cell Mechanics, Phys. Rev. Lett. **108**, 178103 (2012).
[73] D. Zhou, L. Zhang, and X. Mao, Topological Edge Floppy Modes in Disordered Fiber Networks, Phys. Rev. Lett. **120**, 068003 (2018).
[74] J. Notbohm, A. Lesman, P. Rosakis, D. A. Tirrell, and G. Ravichandran, Microbuckling of fibrin provides a mechanism for cell mechanosensing, J. R. Soc. Interface **12**, 20150320 (2015).
[75] B. Lee, X. Zhou, K. Riching, K. W. Eliceiri, P. J. Keely, S. A. Guelcher, A. M. Weaver, and Y. Jiang, A three-dimensional computational model of collagen network mechanics, PLoS ONE **9**, e111896 (2014).
[76] C. P. Broedersz and F. C. Mackintosh, Modeling semiflexible polymer networks, Rev. Mod. Phys. **86**, 995 (2014).
[77] B. Burkel and J. Notbohm, Mechanical response of collagen networks to nonuniform microscale loads, Soft Matter **13**, 5749 (2017).
[78] P. Grimmer and J. Notbohm, Displacement propagation and nonaffinity in collagen networks due to local contraction, J. Biomech. Eng. **13**, 5749 (2017).
[79] N. Wang, J. D. Tytell, and D. E. Ingber, Mechanotransduction at a distance: Mechanically coupling the extracellular matrix with the nucleus, Nat. Rev. Mol. Cell Biol. **10**, 75 (2009).
[80] S. Na, O. Collin, F. Chowdhury, B. Tay, M. Ouyang, Y. Wang, and N. Wang, Rapid signal transduction in living cells is a unique feature of mechanotransduction, Proc. Natl. Acad. Sci. USA **105**, 6626 (2008).
[81] D. S. Bassett, E. T. Owens, M. A. Porter, M. L. Manning, and K. E. Daniels, Extraction of force-chain network architecture in granular materials using community detection, Soft Matter **11**, 2731 (2015).
[82] L. Papadopoulos, M. A. Porter, K. E. Daniels, and D. S. Bassett, Network analysis of particles and grains, arXiv:1708.08080.
[83] W. Han, S. Chen, W. Yuan, Q. Fan, J. Tian, X. Wang, L. Chen, X. Zhang, W. Wei, R. Liu, J. Qu, Y. Jiao, R. H. Austin, and L. Liu, Oriented collagen fibers direct tumor cell intravasation, Proc. Natl. Acad. Sci. USA **113**, 11208 (2016)
[84] C. L. Y. Yeong and S. Torquato, Reconstructing random media, Phys. Rev. E **57**, 495 (1998).
[85] C. L. Y. Yeong and S. Torquato, Reconstructing random media: II. Three-dimensional media from two-dimensional cuts, Phys. Rev. E **58**, 224 (1998).
[86] Y. Jiao, F. H. Stillinger, and S. Torquato, Modeling heterogeneous materials via two-point correlation functions: Basic principles, Phys. Rev. E **76**, 031110 (2007).
[87] Y. Jiao, F. H. Stillinger, and S. Torquato, Modeling heterogeneous materials via two-point correlation functions II: Algorithmic details and applications, Phys. Rev. E **77**, 031135 (2008).
[88] Y. Jiao, F. H. Stillinger, and S. Torquato, A superior descriptor of random textures and its predictive capacity, Proc. Natl. Acad. Sci. USA **106**, 17634 (2009).
[89] C. E. Zachary and S. Torquato, Improved reconstructions of random media using dilation and erosion processes, Phys. Rev. E **84**, 056102 (2011).
[90] Y. Jiao, E. Padilla, and N. Chawla, Modeling and predicting microstructure evolution in lead/tin alloy via correlation functions and stochastic material reconstruction, Acta Mater. **61**, 3370 (2013)
[91] E. Y. Guo, N. Chawla, T. Jing, S. Torquato, and Y. Jiao, Accurate modeling and reconstruction of three-dimensional filamentary structures from two-dimensional micrographs via dilation-erosion method, Mater. Charac. **89**, 33 (2014).
[92] Y. Jiao and N. Chawla, Modeling and charactering anisotropic inclusion orientation in heterogeneous materials via directional cluster function and stochastic reconstruction, J. Appl. Phys. **115**, 093511 (2014).

[93] H. Li, N. Chawla, and Y. Jiao, Reconstruction of heterogeneous materials via stochastic optimization of limited-angle x-ray tomographic projections, Scr. Mater. **86**, 48 (2014).

[94] S. Chen, H. Li, and Y. Jiao, Dynamic reconstruction of heterogeneous materials and microstructure evolution, Phys. Rev. E **92**, 023301 (2015).

[95] S. Chen, A. Kirubanandham, N. Chawla, and Y. Jiao, Stochastic multi-scale reconstruction of 3D microstructure consisting of polycrystalline grains and second-phase particles from 2D micrographs, Metal. Mater. Trans. A **47**, 1440 (2015).

[96] H. Li, S. Kaira, J. Mertens, N. Chawla, and Y. Jiao, Accurate stochastic reconstruction of heterogeneous microstructures by limited x-ray tomographic projections, J. Microsc. **264**, 339 (2016).

[97] S. Kirkpatrick, C. D. Gelatt, and M. P. Vecchi, Optimization by simulated annealing, Science **220**, 671 (1983).

[98] J. Steinwachs, C. Metzner, K. Skodzek, N. Lang, I. Thievessen, C. Mark, S. Manster, K. E. Aifantis, and B. Fabry, Three-dimensional force microscopy of cells in biopolymer networks, Nat. Method **13**, 171 (2015).